Continuous surface potential versus voltage equation of intrinsic surrounding-gate MOSFETs and analytic solution from accumulation to strong inversion region*

He Jin(何进)[1,2,†], Zheng Rui(郑睿)[2], Zhang Lining(张立宁)[2], Zhang Jian(张健)[2], Lin Xinnan(林信南)[2] , and Chan Mansun(陈文新)[1]

(1 Department of Electronics and Computer Engineering, Hong Kong University of Science & Technology, Hong Kong, China)
(2 Micro & Nano Electric Device and Integrated Technology Group, Key Laboratory of Integrated Microsystems, Peking University, Shenzhen Graduate School,Shenzhen 518055, China)

Abstract: A continuous surface potential versus voltage equation is proposed and then its solution is further discussed for a long channel intrinsic surrounding-gate (SRG) MOSFET from the accumulation to strong inversion region. The original equation is derived from the exact solution of a simplified Poisson equation and then the empirical correction is performed from the mathematical condition required by the continuity of the solution, which results in a continuous surface potential versus voltage equation, allowing the surface potential and the related derivatives to be described by an analytic solution from the accumulation to strong inversion region and from linear to the saturation region accurately and continuously. From these results, the dependences of surface potential and centric potential characteristics on device geometry are analyzed and the results are also verified with the 3-D numerical simulation from the aspect of accuracy and continuity tests.

Key words: non-classical CMOS; surrounding-gate MOSFETs; device physics; surface potential; accuracy; continuity issue

DOI: 10.1088/1674-4926/31/6/064001 **PACC:** 7340Q **EEACC:** 2560B; 2570D

1. Introduction

According to ITRS the traditional single-gate bulk CMOS will hit its scaling limit in several years due to severe short-channel effects and ultra-thin gate oxide tunneling[1]. In order to extend the scalability of CMOS technology beyond the 22 nm technology generation many non-classical multi-gate MOSFET configurations have been proposed[2–5]. Among them, the surrounding-gate (SRG) MOSFETs demonstrate the best control of short-channel effects, thus, it can be scaled to the shortest channel length for a given gate oxide thickness. To implement the potential advantage of this device in future generation CMOS integrated circuits, compact models will be required for the electrical circuit simulation and design. For these applications, a complete SRG MOSFET model requires an accurate and continuous mathematical formulation to describe the device characteristics.

Surface-potential-based models are becoming mainstream either for bulk MOSFETs or non-classical CMOS devices in the compact modelling community, as they include a more physical and accurate description of the MOS (metal–oxide–semiconductor) transistor behavior[6–10]. The complete surface potential versus voltage equation of a bulk MOS transistor was initiated by Sah and Pao in 1966, and then finally clarified and unified by Sah, He and PSP groups from different device physics routes[11–17]. The electrostatic analysis and the corresponding surface potential versus voltage equation of the double-gate (DG) MOSFET have also been well studied and established[18–23]. Various compact models for the surrounding-gate (SRG) MOSFET such as potential-based models, charge-based models and carrier-based models and the complete surface potential-based model have been presented in Refs. [24–35]. They have different intermediate variables and differ in their computation efficiency. On the other hand, the continuity of the surface potential versus voltage equation is a key factor for the compact model used in circuit simulators in order to maintain the simulation convergence. Recently, discontinuity problems of the surface potential versus voltage equation of the bulk MOSFETs which strongly degrade the compact model convergence and computation efficiency have been found and finally amended by several group works[12–15]. In Ref. [23] a rigorous surface potential solution for symmetric DG MOSFETs is obtained which is naturally continuous but depends on an iterative algorithm. However, the discontinuity issue of the electrostatic analysis of the SRG MOSFET has never been mentioned and discussed in the previous models[24–35] although it is very important for the SRG MOSFET model application. Under such a background, a continuous surface potential versus voltage equation and its analytical solution for the SRG MOSFETs is desired for the SRG MOSFET compact model development.

Based on the previous work[32–35], a continuous surface potential versus voltage equation of intrinsic cylindrical SRG

* Project supported by the National Natural Science Foundation of China (No. 60876027), the Competitive Earmarked Program from the Research Grant Council of Hong Kong SAR, China (No.HKUST6289/04E), the Industry, Education and Academy Cooperation Program of Guangdong Province, China (No. 2009B090300318), and the Fundamental Research Project of Shenzhen Science & Technology Foundation, China (No. JC200903160353A).

† Corresponding author. Email: eejinhe@ust.hk

Received 1 December 2009, revised manuscript received 18 January 2010

© 2010 Chinese Institute of Electronics

MOSFETs from the accumulation to strong inversion region is proposed from the continuity property, together with an analytical algorithm in this paper. These two points are the major contributions of this work. From it, the surface potential continuity and derivative characteristics of SRG MOSFETs are analyzed. Moreover, the theoretical surface potential and centric potential predictions are compared with a 3-D numerical simulation and good agreements are found between them for wide ranges of bias parameters, proving the accuracy of the presented surface potential equation and its solution for the SRG compact modelling application.

2. Electrostatic analysis of SRG MOSFETs

In order to calculate the potential distribution along the radius direction, one may follow the usual procedure of the bulk MOSFET analysis and start with the Poisson equation under the gradual-channel approximation (GCA):

$$\frac{\mathrm{d}^2\phi}{\mathrm{d}r^2}+\frac{1}{r}\frac{\mathrm{d}\phi}{\mathrm{d}r}=-\frac{\rho}{\varepsilon_{\mathrm{si}}}, \tag{1}$$

with the charge concentration expressed as: $\rho = q\left(p+N_{\mathrm{d}}-n-N_{\mathrm{a}}\right)$. Here all the symbols have their common meanings.

Since an intrinsic or lightly doped body is preferred in the SRG-MOSFETs, we can neglect the effects of the impurity charge due to their small magnitude, thus

$$N_{\mathrm{a}}=N_{\mathrm{d}}=0. \tag{2}$$

The charge term is simplified as:

$$\rho=q\left(p-n\right). \tag{3}$$

Based on Boltzmann statistics, the electron and hole concentrations can be expressed as

$$n=n_{\mathrm{i}}\exp\frac{q(\phi-V_{\mathrm{ch}})}{kT}, \tag{4}$$

$$p=n_{\mathrm{i}}\exp\left(-\frac{q\phi}{kT}\right). \tag{5}$$

Note that the hole quasi-Fermi-potential is taken as the reference point because only an N-type SRG MOSFET is considered here.

The Poisson equation thus takes the following form:

$$\frac{\mathrm{d}^2\phi}{\mathrm{d}r^2}+\frac{1}{r}\frac{\mathrm{d}\phi}{\mathrm{d}r}=\frac{kT}{qL_{\mathrm{i}}^2}\left[\exp\frac{q\left(\phi-V_{\mathrm{ch}}\right)}{kT}-\exp\frac{-q\phi}{kT}\right], \tag{6}$$

with the boundary conditions:

$$\frac{\mathrm{d}\phi}{\mathrm{d}r}(r=0)=0,\quad -\frac{\mathrm{d}\phi}{\mathrm{d}r}(r=R)=E_{\mathrm{s}}, \tag{7}$$

and

$$\phi(r=0)=\phi_0,\quad \phi(r=R)=\phi_{\mathrm{s}}, \tag{8}$$

where ϕ_{s} and E_{s} are the surface potential and electric field at the silicon and gate oxide interface, ϕ_0 is the centric potential and $L_{\mathrm{i}}^2=1/(q^2n_{\mathrm{i}}/kT\varepsilon_{\mathrm{si}})$.

The analytic solution of Eq. (6) with conditions of Eqs. (7) and (8) is physical and continuous since it includes both hole and electron item contributions. However, it is not a trial equation without any analytic solution. Thus, the previous works had to solve the simplified formulation of Eq. (6) with a single electron or hole item and then presented regional solutions for a single electron or hole item, respectively[25–28, 32–34]. As a result, the previous solutions are only valid above the flat-band point or into the accumulation. Thus, it is this work's aim to get a continuous surface potential equation and its global solution based on the previous region solutions.

For SRG-MOSFET operation above the flat-band point, the electron dominates the charge term in Eq. (6)[25–28, 32–34], and Equation (6) is simplified as

$$\frac{\mathrm{d}^2\phi}{\mathrm{d}r^2}+\frac{1}{r}\frac{\mathrm{d}\phi}{\mathrm{d}r}=\frac{kT}{qL_{\mathrm{i}}^2}\exp\frac{q\left(\phi-V_{\mathrm{ch}}\right)}{kT}. \tag{9}$$

We would like to point out in advance that such a simplification of the Poisson equation, thus, the solution of Eq. (9), will result in a discontinuity near the flat-band point, which has never been noted and discussed in the previous literature. This problem will be discussed and then fixed in the following continuous surface potential versus voltage equation.

Equation (9) is analytically solved[34]:

$$\frac{q\left(V_{\mathrm{gs}}-\Delta\varphi-\phi_{\mathrm{s}}\right)}{kT}\left[\frac{1}{R}+\frac{qC_{\mathrm{ox}}\left(V_{\mathrm{gs}}-\Delta\varphi-\phi_{\mathrm{s}}\right)}{4\varepsilon_{\mathrm{si}}kT}\right]=\frac{\varepsilon_{\mathrm{si}}}{2L_{\mathrm{i}}^2C_{\mathrm{ox}}}\exp\frac{q\left(\phi_{\mathrm{s}}-V_{\mathrm{ch}}\right)}{kT}, \tag{10}$$

where $C_{\mathrm{ox}}=\varepsilon_{\mathrm{ox}}/[R\ln(1+t_{\mathrm{ox}}/R)]$ and $\Delta\varphi$ is the work-function difference between gate and intrinsic silicon.

Due to the multiple root characteristics of Eqs. (10) and (11) with respect to V_{gs}–$\Delta\varphi$, we make use of the solution procedure of a general quadratic equation to derive a SRG MOSFET surface potential versus voltage equation with a single root from the physical meaning of the solution, as shown in Eq. (11):

$$\frac{q\left(V_{\mathrm{gs}}-\Delta\varphi-\phi_{\mathrm{s}}\right)}{kT}=\frac{2\varepsilon_{\mathrm{si}}}{RC_{\mathrm{ox}}}\sqrt{1+\frac{R^2}{2L_{\mathrm{i}}^2}\exp\frac{q\left(\phi_{\mathrm{s}}-V_{\mathrm{ch}}\right)}{kT}}-\frac{2\varepsilon_{\mathrm{si}}}{RC_{\mathrm{ox}}}. \tag{11}$$

Equations (10) and (11) is a surface potential equation of the SRG MOSFET based on a fully rigorous solution of the simplified Poisson equation (9) above the flat-band point. We note that Equations (10) and (11) cannot stand for the electrostatic potential when the device operates very close to the flat-band point due to the simplification of the Poisson equation, thus the calculated field and potential cannot pass through the flat-band point with changing gate voltage. This problem is fixed by adding a new term $-\exp\frac{-qV_{\mathrm{ch}}}{kT}$ to the right-hand side of Eqs. (10) and (11) as shown in Eq. (12).

$$\frac{q\left(V_{\mathrm{gs}}-\Delta\varphi-\phi_{\mathrm{s}}\right)}{kT}=\frac{2\varepsilon_{\mathrm{si}}}{RC_{\mathrm{ox}}}\times\sqrt{1+\frac{R^2}{2L_{\mathrm{i}}^2}\left(\exp\frac{q\left(\phi_{\mathrm{s}}-V_{\mathrm{ch}}\right)}{kT}-\exp\frac{-qV_{\mathrm{ch}}}{kT}\right)}-\frac{2\varepsilon_{\mathrm{si}}}{RC_{\mathrm{ox}}}. \tag{12}$$

In modelling the capacitance–voltage characteristics of SRG MOSFETs, such as calculating the capacitances related to ϕ_s, the first-order differential of ϕ_s is needed. However, Equation (12) still results in discontinuity when it is differentiated with gate voltage. Based on the mathematical condition of the continuous derivative of the surface potential with respect to the terminal voltage, Equation (12) is further modified as

$$\frac{q\left(V_{gs}-\Delta\varphi-\phi_s\right)}{kT}=\frac{2\varepsilon_{si}}{RC_{ox}}\times\sqrt{1+\frac{R^2}{2L_i^2}\left[\exp\frac{q\left(\phi_s-V_{ch}\right)}{kT}-\left(1+\frac{q\phi_s}{kT}\right)\exp\frac{-qV_{ch}}{kT}\right]}-\frac{2\varepsilon_{si}}{RC_{ox}}. \quad (13)$$

For the SRG-MOSFET operating in the accumulation region, holes dominate the charge concentration in the channel. In this case, the derivation is straightforward as done above. Firstly Equation (6) is simplified as

$$\frac{d^2\varphi}{dr^2}+\frac{1}{r}\frac{d\varphi}{dr}=-\frac{kT}{qL_i^2}\exp\frac{-q\varphi}{kT}. \quad (14)$$

Then following a similar routine, the solution of Eq. (14) is obtained as

$$\frac{q\left(V_{gs}-\Delta\varphi-\phi_s\right)}{kT}\left[\frac{1}{R}-\frac{qC_{ox}\left(V_{gs}-\Delta\varphi-\phi_s\right)}{4\varepsilon_{si}kT}\right]=-\frac{\varepsilon_{si}}{2L_i^2C_{ox}}\exp\frac{-q\phi_s}{kT}, \quad (15)$$

$$\frac{q\left(V_{gs}-\Delta\varphi-\phi_s\right)}{kT}=\frac{2\varepsilon_{si}}{RC_{ox}}-\frac{2\varepsilon_{si}}{RC_{ox}}\sqrt{1+\frac{R^2}{2L_i^2}\exp\frac{-q\phi_s}{kT}}. \quad (16)$$

Again, Equations (15) and (16) is the solution of a simplified Poisson equation beyond the flat-band point. To ensure that the surface potential passes through the flat-band point and the derivative is continuous, Equation (16) is modified similarly to Eq. (11):

$$\frac{q\left(V_{gs}-\Delta\varphi-\phi_s\right)}{kT}=\frac{2\varepsilon_{si}}{RC_{ox}}-\frac{2\varepsilon_{si}}{RC_{ox}}\sqrt{1+\frac{R^2}{2L_i^2}\left(\exp\frac{-q\phi_s}{kT}-1\right)}, \quad (17)$$

$$\frac{q\left(V_{gs}-\Delta\varphi-\phi_s\right)}{kT}=\frac{2\varepsilon_{si}}{RC_{ox}}-\frac{2\varepsilon_{si}}{RC_{ox}}\sqrt{1+\frac{R^2}{2L_i^2}\left(\exp\frac{-q\phi_s}{kT}+\frac{q\phi_s}{kT}-1\right)}. \quad (18)$$

In bulk MOSFETs, a single equation is obtained in terms of the surface potential from the accumulation to strong inversion region. For intrinsic SRG MOSFETs the corresponding equation which is valid in all operation regions is also obtained by combining Eqs. (12, 17) and (13, 18), respectively:

$$\frac{q\left(V_{gs}-\Delta\varphi-\phi_s\right)}{kT}+\frac{\mathrm{sgn}(\phi_s)2\varepsilon_{si}}{C_{ox}R}=\frac{\mathrm{sgn}(\phi_s)2\varepsilon_{si}}{C_{ox}R}\sqrt{1+\frac{R^2\theta}{2L_i^2}\left\{\exp\left[\mathrm{sgn}\left(\phi_s\right)\frac{q\phi_s}{kT}\right]-1\right\}}, \quad (19)$$

$$\frac{q\left(V_{gs}-\Delta\phi-\phi_s\right)}{kT}+\frac{\mathrm{sgn}(\phi_s)2\varepsilon_{si}}{C_{ox}R}=\frac{\mathrm{sgn}(\phi_s)2\varepsilon_{si}}{C_{ox}R}\times\sqrt{1+\frac{R^2\theta}{2L_i^2}\left\{\exp\left[\mathrm{sgn}\left(\phi_s\right)\frac{q\phi_s}{kT}\right]-\mathrm{sgn}(\phi_s)\frac{q\phi_s}{kT}-1\right\}}, \quad (20)$$

where $\mathrm{sgn}(\varphi_s)$ is the signum function that returns 1 if the band bending is above or at the flat-band region and -1 when the band bending is below the flat-band region. θ is the quasi-Fermi-potential factor:

$$\theta=\begin{cases}\exp(-qV_{ch}/kT), & \text{above flat-band point,}\\ 1, & \text{flat-band or accumulation.}\end{cases} \quad (21)$$

Equations (19) and (20) are valid for all bias conditions. We would like to further point out that Eq. (19) is continuous for the surface potential and charge but it is not for the derivative of the surface potential with respect to the gate voltage from the accumulation to strong inversion region. In contrast, Equation (20) is infinitely continuous either for a surface potential and charge or for any order derivative of the related physical quantities.

3. Analytic solution to the surface potential equation

An empirical continuous surface potential equations (19) and (20) is proposed to realize its smooth transition through the flat-band point with changing gate voltage. However, the problem is that Equations (19) and (20) is an implicit transcendental equation just like other surface potential based models. For a bulk MOSFET with a uniformly doped substrate, the complete surface potential equation was solved analytically in Refs. [16, 17]. Following similar methods, the authors presented explicit continuous models for SRG MOSFETs in Refs. [30, 31] for the equivalent form of the surface potential equation to Eqs. (10) and (11). Here a method similar to that in Ref. [16] is proposed to give an analytic surface potential solution.

From careful observation of the implicit equations (19) and (20), we find that the silicon film radius plays a unique role. For an infinitely large silicon film radius which implies an intrinsic bulk MOSFET, Equations (19) and (20) becomes

$$\frac{C_{ox}(V_{gs}-\Delta\varphi-\phi_s)}{\sqrt{2n_i\varepsilon_{si}kT}}=\mathrm{sgn}\left(\phi_s\right)\sqrt{\theta}\exp\left[\mathrm{sgn}\left(\phi_s\right)\frac{q\phi_s}{2kT}\right], \quad (22)$$

where we neglect the added $[-\mathrm{sgn}(\phi_s)\,\frac{q\phi_s}{kT}-1]$ terms, which is reasonable because they only come into effect when the operation region is very close to the flat-band point. Equation (22) is similar to the Poisson equation solution of the intrinsic bulk MOSFET given by Ortiz–Conde[36]. Thus, it has an exact solution based on Lambert-W function formulation

$$\phi_{s0}=V_{gs}-\Delta\varphi-\mathrm{sgn}\left(\phi_s\right)\frac{2kT}{q}W_0\times\left\{\frac{1}{C_{ox}}\sqrt{\frac{2\varepsilon_{si}qn_i\theta}{kT}}\exp\left[\mathrm{sgn}\left(\phi_s\right)\frac{q(V_{gs}-\Delta\varphi)}{2kT}\right]\right\}. \quad (23)$$

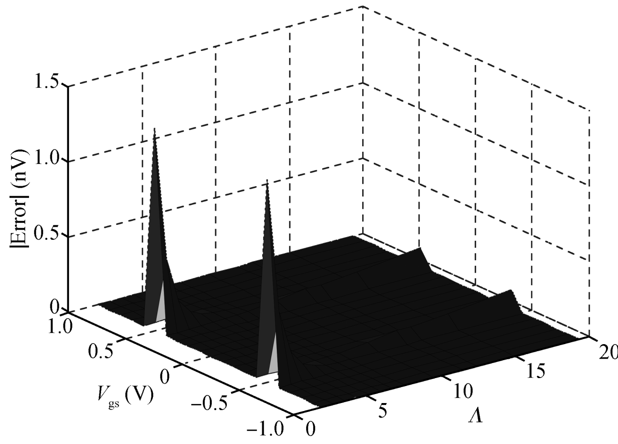

Fig. 1. Absolute error of the analytical algorithm for surface potential equation (20) compared with numerically solved results as functions of gate voltage and geometry parameters.

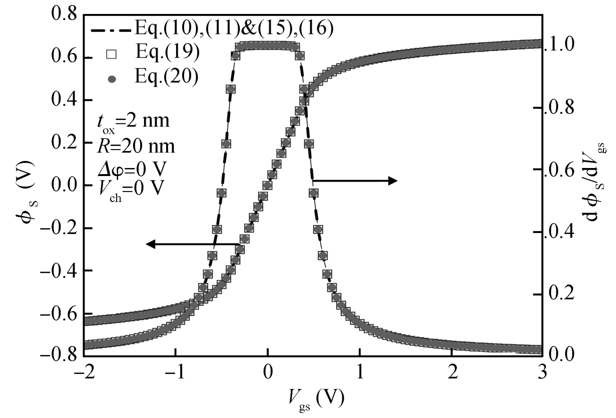

Fig. 2. Comparisons of the surface potential and its derivative between three equation pairs for a wide gate voltage range.

Equation (23) is used as a global initial guess of the surface potential for all the operation regions. Then a second order correction function is used to achieve higher accuracy. Here the correction function to Eq. (20) is demonstrated.

$$\phi_s = \phi_{s0} - \frac{f/\partial f}{1 - 0.5 f \partial^2 f/\partial f/\partial f}, \quad (24)$$

where

$$f = \left[\frac{q\left(V_{gs} - \Delta\varphi - \phi_s\right)}{kT} + \mathrm{sgn}(\phi_s)\frac{2\varepsilon_{si}}{RC_{ox}}\right]^2 - \left(\frac{2\varepsilon_{si}}{RC_{ox}}\right)^2 \times \left[1 + \frac{R^2\theta}{2L_i^2}\left\{\exp\left[\mathrm{sgn}(\phi_s)\frac{q\phi_s}{kT}\right] - \mathrm{sgn}(\phi_s)\frac{q\phi_s}{kT} - 1\right\}\right], \quad (25)$$

$$\partial f = -2\left[\frac{q\left(V_{gs} - \Delta\varphi - \phi_s\right)}{kT} + \mathrm{sgn}(\phi_s)\frac{2\varepsilon_{si}}{RC_{ox}}\right] - \mathrm{sgn}(\phi_s) \times \left(\frac{2\varepsilon_{si}}{RC_{ox}}\right)^2 \frac{R^2\theta}{2L_i^2}\left\{\exp\left[\mathrm{sgn}(\phi_s)\frac{q\phi_s}{kT}\right] - 1\right\}, \quad (26)$$

$$\partial^2 f = 2 - \left(\frac{2\varepsilon_{si}}{RC_{ox}}\right)^2 \frac{R^2\theta}{2L_i^2} \exp\left[\mathrm{sgn}(\phi_s)\frac{q\phi_s}{kT}\right]. \quad (27)$$

After two correction procedures, the obtained surface potential is accurate enough for application in compact models. To solve the initial solution from Eq. (23) with the Lambert-W function, one exponent and three logarithms are included[37]. For the correction function (24), two exponents are included. In total, three exponents and three logarithms are involved in the preceding algorithm. Figure 1 demonstrates the absolute error of the analytical surface potential solution of Eq. (20) compared with the Newton-Raphson iterative result. The errors are sensitive to the geometry of the device ($\Lambda = R/t_{ox}$ in Fig. 1), as shown in Fig. 1, since the initial solution Eq. (23) assumes infinitely large radii. As shown in the figure, the maximum absolute error is within 1 nV order for a reasonable range of geometry and bias parameters.

Note that in Ref. [32] an explicit solution for the SRG MOSFET is presented. However, the starting point in Ref. [32] is Eq. (9), thus the discontinuity problems of the surface potential versus voltage equation are not addressed. Here in this work the emphasis is on finding one feasible approach to solve this problem. It is also found that the method in Ref. [16] to solve the input voltage equation in a bulk MOSFET is applicable to Eq. (23) of an undoped SRG MOSFET here.

4. Results and discussion

The continuity of the equation and thus the model of a semiconductor device is an essential feature for ULSI circuit simulation, which ensures simulation convergence. For the surface potential equation of an SRG MOSFET and the relative derivative, it is also true for the model application. We first discuss the results of three pairs of equations, Eqs. (10), (11) & (15), (16), Eqs. (12) & (17) (i.e. Eq. (19)), and Eqs. (13) & (18) (i.e. Eq. (20)). Figure 2 plots the calculated φ_s (left) and dϕ_s /dV_{gs} (right) versus V_{gs} for a wide gate voltage range from these three equations. The solid circles denote the analytically solved results from Eq. (20) while the open squares correspond to the solution of Eq. (19); lines are the results from the equation pair of Eqs. (10), (11) and (15), (16) both numerically calculated. As shown in Fig. 2, the results from the three surface potential equations match well in such a gate voltage range and step and seem to show no differences from each other. In the operation region far from the flat-band point, the difference between Eqs. (10), (11), (15), (16) and Eq. (20) is negligible. This result, on one hand, indicates that the modifications in Eqs. (19) and (20) are reasonable; on the other hand, it suggests that the drawbacks of Eqs. (10), (11), (15), (16) and Eq. (19) need to be observed in a refined gate voltage scope.

Figure 3 demonstrates the calculated results of the ϕ_s versus V_{gs} curve near the flat-band point in a refined gate voltage range. Again Equation (20) is solved analytically with the proposed algorithm and results from the other two equations are numerically obtained. As shown in Fig. 3, Equations (10), (11) and (15), (16) result in a discontinuity problem of the surface potential versus gate voltage, thus the calculated surface potential cannot pass through the flat-band point smoothly below and above it. This problem is fixed by adding a $-\exp\frac{-qV}{kT}$ term to modify Eq. (10), (11) or (15), (16) respectively, evaluating Eq. (19). It is found that the surface potential calculated using

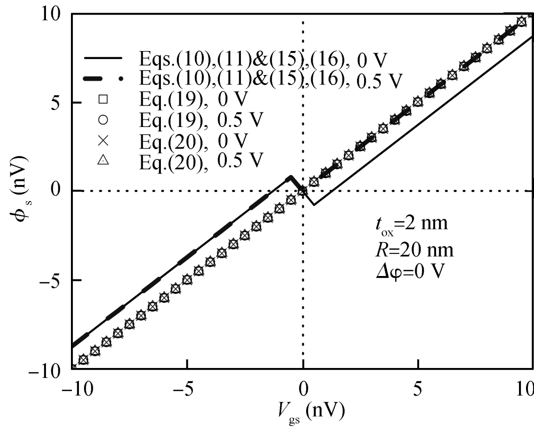

Fig. 3. Comparisons of ϕ_s versus V_{gs} near the flat band-point between three equation pairs for different V_{ch}, in a refined gate voltage scope, showing a discontinuity of the surface potential from Eqs. (10), (11) and (15), (16) pairs.

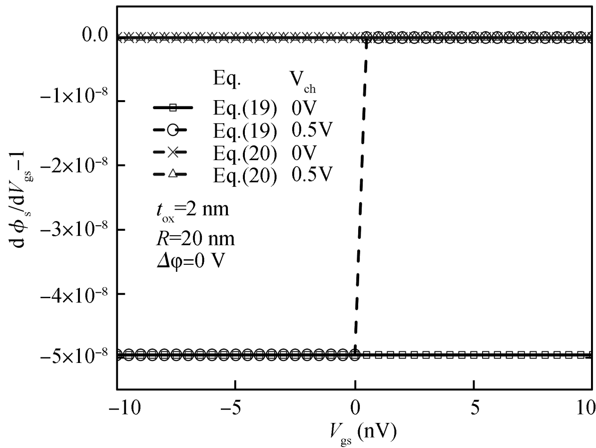

Fig. 4. Comparisons of $d\phi_s/dV_{gs}-1$ versus V_{gs} near the flat-band point between Eqs. (19) and (20), showing the discontinuity of the surface potential derivative from Eq. (19).

(19) can pass through the flat-band point even considering zero V_{ch}. In addition, we also note that further modification on Eq. (19), i.e. Eq. (20), also demonstrates its own continuous characteristics from below to above the flat-band point. Moreover, Equation (20) fits the result of Eq. (19) so well in this refined gate voltage scope that the distinction between them is not significantly illustrated. The difference, however, can be observed from the difference between the derivatives from Eqs. (20) and (19) as shown in Fig. 4.

Figure 4 plots $d\phi_s / dV_{gs}$ from the numerically solved Eq. (19) (represented by squares and circles) and the analytically evaluated Eq. (20) (represented by crosses and triangles). As expected, Equation (19) results in a discontinuous derivative of the surface potential with respect to gate voltage close to the flat-band point when $V_{ch} \neq 0$ although it results in a continuous surface potential. This result indicates that Equation (19) cannot be used to predict the capacitance-voltage characteristics of SRG-MOSFETs. In order to fix this flaw, Equation (20) has to be used and the resultant derivative of the surface potential with respect to the gate voltage is smooth when passing the flat-band point either for zero and non-zero quasi-Fermi potentials as demonstrated in Fig. 4. In fact, Equation (20) fixes all the discontinuity problems and its result is infinitely continuous.

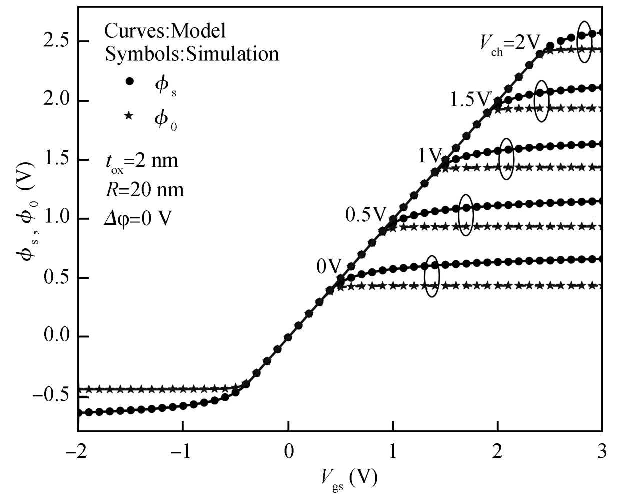

Fig. 5. Surface potential φ_s and centric potential φ_0 versus V_{gs} obtained from the surface potential equation (lines) for different V_{ch} and 3-D simulation (symbols).

The continuity of the surface potential and its derivative is a necessary rather than sufficient condition for the utility of the surface potential versus voltage equation for SRG-MOSFET modelling. In practice, the accuracy of the presented surface potential equation and its derivatives is a more stringent test for SRG-MOSFET device physics analysis. All equation predictions in the following discussion are based on the analytically solved Eq. (20), and the corresponding centric potentials (φ_0) are obtained directly as functions of ϕ_s [34]. On the other hand, the numerical simulation is performed from the commercial device simulator Sentaurus[38].

Figure 5 is a comparison of the result between the surface potential and the centric potential versus gate voltage curves of the 3-D simulation (symbols) and the surface potential equation prediction (lines) for different quasi-Fermi-potentials. It is easily seen that the surface potential equation prediction agrees with the 3-D simulation very well: the error is within a range of less than 0.15%, indicating the accuracy of Eq. (20). As in the bulk MOSFETs, the surface potential operation region is divided into two significantly different regions above the flat-band point: one is the sub-threshold region where the surface potential is almost a linear function of the gate voltage, and the other is the strong inversion region where the surface potential saturates gradually. Similarly, the quasi-Fermi potential comes into effect only when the SRG-MOSFET operation goes into the strong inversion region. We find from Fig. 5 that the centric potential merges with the surface potential in the sub-threshold region while it diverges from the surface potential when it enters both the strong inversion and the strong accumulation regions where it becomes almost flat, e.g. saturates into a constant value. This saturation centric potential can be explained by the argument of the logarithmic items in its expression[34]. For example, the logarithmic function requires the argument in it to be larger than zero, thus, it results in the maximum centric

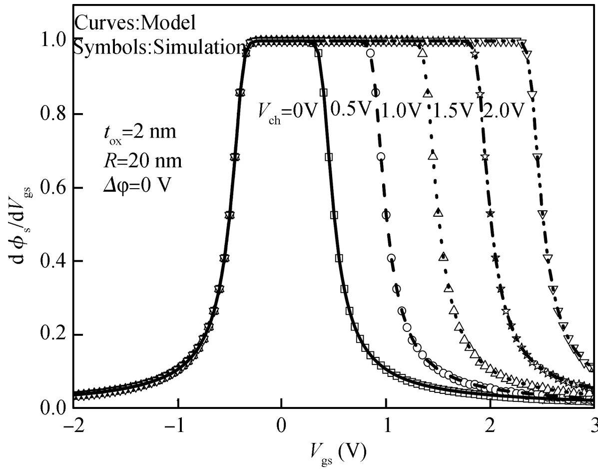

Fig. 6. Surface potential φ_s derivatives versus V_{gs} obtained from the surface potential equation for different V_{ch} in comparison with 3-D simulation.

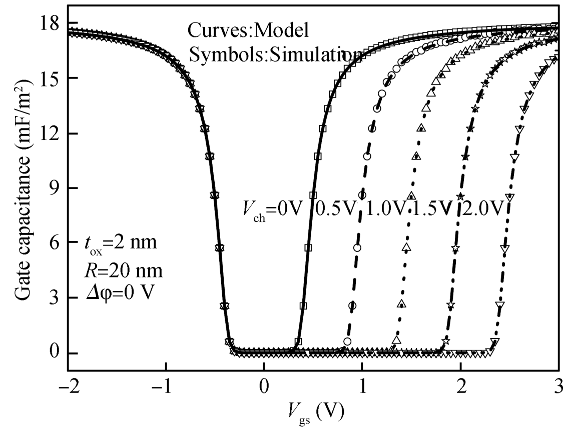

Fig. 7. Gate capacitance versus V_{gs} from the surface potential equation for different V_{ch} in comparison with 3-D simulation.

potential

$$\phi_{0,\max} = \frac{kT}{q}\ln\theta + \operatorname{sgn}(\phi_s)\frac{kT}{q}\ln\frac{8L_i^2}{R^2}. \qquad (28)$$

As stated above, one stringent test on the SRG-MOSFET surface potential equation is the continuity and high precision of the surface potential derivatives with respect to the gate voltage. Figure 6 shows a comparison between the surface potential derivatives of the surface potential equation and the 3-D simulation for different quasi-Fermi-potentials. We find that not only does the equation prediction remain continuous and smooth in the whole SRG-MOSFET operation region from the accumulation, thorough the flat-band point and sub-threshold, and finally to the strong inversion region, but it also matches the 3-D numerical simulation very well. These results indicate that the accuracy of the presented surface potential equation and its derivative is satisfactory for the SRG-MOSFET electrostatic analysis and performance test.

Precision of the gate capacitance from the presented surface potential equation is highly desirable in SRG-MOSFET small signal analysis from the accumulation to the strong inversion region. Once the surface potential and its derivative are obtained, the corresponding gate-capacitance is easily obtained with the following formulation:

$$\frac{C_{gg}}{C_{ox}} = \frac{dQ_g}{C_{ox}dV_{gs}} = 1 - \frac{d\phi_s}{dV_{gs}}. \qquad (29)$$

Figure 7 plots a comparison between the gate capacitance curves of the surface potential equation calculation and the 3-D simulation for different quasi-Fermi-potentials. As expected, not only does the equation predicted gate capacitance remain continuous and smooth in the whole SRG-MOSFET operation region, but it again matches the 3-D numerical simulation very well.

5. Conclusions

In summary, an empirically continuous and physics based surface potential versus voltage equation is presented in this paper for a long intrinsic channel (lightly doped) surrounding-gate (SRG) MOSFET from the accumulation to strong inversion region and its analytical solution is also discussed. The equation is derived from the Poisson equation and then amended with the appropriate mathematical condition for the continuity of the surface potential and its derivative. From these results, the surface potential and its derivative property of an SRG MOSFET are discussed and the results are also compared with the 3-D simulation. The excellent agreement between them suggests that the proposed empirical surface potential equation and its analytical solution may provide a solid basis for the surface potential based compact model development of SRG MOSFETs.

References

[1] ITRS. International Technology Roadmap for Semiconductors 2005. http://www.itrs.org
[2] Frank D J, Dennard R H, Nowak E, et al. Device scaling limits of Si MOSFETs and their application dependencies. Proc IEEE, 2001, 89(3): 259
[3] Colinge J P. Multiple-gate SOI MOSFETs. Solid State Electron, 2004, 48(6): 897
[4] Park J, Colinge J P, Diaz C H. Pi-gate SOI MOSFET. IEEE Electron Device Lett, 2001, 22(8): 405
[5] Chen Y, Luo J. A comparative study of double-gate and surrounding-gate MOSFETs in strong inversion and accumulation using an analytical model. Proc Int Conf Modeling and Simulation of Microsystems, 2001: 546
[6] Joardar K, Gullapalli K K, McAndrew C C, et al. An improved MOSFET model for circuit simulation. IEEE Trans Electron Devices, 1998, 45(1): 134
[7] HISIM. http://www.starc.jp/kaihatu/pdgr /hisim/index-e.html
[8] MOS-11. http://www.semiconductors.Philips.com/Philips_Models /mos_models
[9] PSP model. http://www.semiconductors.Philips.com/Philips_ Models
[10] He J. Benchmark test on conventional surface potential based charge-shee models and advanced PUNSIM development. Proc Workshop on Compact Modeling, 2005: 390
[11] Sah C T, Pao H C. The effects of fixed bulk charge on the characteristics of metal–oxide–semiconductor transistor. IEEE Trans Electron Devices, 1966, 13(4): 393
[12] McAndrew C C, Victory J. Accuracy of approximations in MOSFET charge models. IEEE Trans Electron Devices, 2002, 49(1):

72
[13] Sah C T. A history of MOS transistor compact modeling. Proc Workshop on Compact Modeling, 2005: 347
[14] He J, Zhang X, Wang Y. Comments on 'modeling MOSFET surface capacitance behavior under non-equilibrium'. Solid State Electron, 2006, 50(2): 259
[15] Wu W, Chen T L, Gildenblat G, et al. Physics-based mathematical conditioning of the MOSFET surface potential equation. IEEE Trans Electron Devices, 2004, 51(7): 1196
[16] He J. A physical-based analytical solution to the MOSFET surface potential from accumulation to strong-inversion region. IEEE Trans Electron Devices, 2006, 53(9): 2008
[17] Gildenblat G, Wang H, Chen T L, et al. SP: an advanced surface-potential-based compact MOSFET model. IEEE J Solid-State Circuits, 2004, 39(9): 1394
[18] Taur Y. An analytical solution to a double-gate MOSFET with undoped body. IEEE Electron Device Lett, 2000, 21(5): 245
[19] Taur Y. Analytic solutions of charge and capacitance in symmetric and asymmetric double-gate MOSFET. IEEE Trans Electron Devices, 2001, 48(12): 2861
[20] Ortiz-Conde A, Garcia Sonchez F J, Malobabic S. Analytic solution of the channel potential in undoped symmetric dual-gate MOSFETs. IEEE Trans Electron Devices, 2005, 52(7): 1669
[21] Shi X, Wong M. Analytical solutions to the one–dimensional oxide–silicon–oxide system. IEEE Trans Electron Devices, 2003, 50(8): 1793
[22] Shangguan W Z, Zhou X, Chandrasekaran K, et al. Surface-potential solution for generic undoped MOSFETs with two gates. IEEE Trans Electron Devices, 2007, 54(1): 169
[23] Zhou X, Zhu Z M, Rustagi S C, et al. Rigorous surface-potential solution for undoped symmetric double-gate MOSFETs considering both electrons and holes at quasi nonequilibrium. IEEE Trans Electron Devices, 2008, 55(2): 616
[24] Jang S L, Liu S S. An analytical surrounding gate MOSFET model. Solid State Electron, 1998, 42(5): 721
[25] Jiménez D, Sáenz J J, Iñíguez B, et al. Continuous analytical current–voltage model for surrounding-gate MOSFETs. IEEE Electron Device Lett, 2004, 25(8): 571
[26] Iñíguez B, Jiménez D, Riog J, et al. Explicit continuous model for long channel undoped surrounding-gate MOSFETs. IEEE Trans Electron Devices, 2005, 52(8): 1868
[27] He J, Zhang X, Zhang G, et al. A carrier-based DCIV model for long channel undoped cylindrical surrounding-gate MOSFETs. Solid State Electron, 2006, 50(3): 416
[28] He J, Chan M. Physics based analytical solution to undoped cylindrical surrounding-gate (SRG) MOSFETs. Proc 5th Int Caracas Conf on Devices, Circuits and Systems, 2004: 26
[29] Oh S H, Monore D, Hergenrother J M. Analytical description of short-channel effects in fully-depleted double-gate and cylindrical, surrounding-gate MOSFETs. IEEE Electron Devices Lett, 2000, 21(9): 445
[30] Auth C P, Plummer J D. Scaling theory for cylindrical, fully-depleted, Surrounding-gate MOSFETs. IEEE Electron Devices Lett, 1997, 18(2): 74
[31] Endoh T, Nakamura T, Masuoka F. An accurate model of fully-depleted surrounding gate transistor. IEICE Trans Electron, 1994, E80-C(7): 905
[32] Yu B, Lu H, Liu M, et al. Explicit continuous models for double-gate and surrounding-gate MOSFETs. IEEE Trans Electron Devices, 2007, 54(10): 2715
[33] Lu H, Yu B, Taur Y. A unified charge model for symmetric double-gate and surrounding-gate MOSFETs. Solid State Electron, 2008, 52(1): 67
[34] Wei B, He J, Tao Y, et al. An analytic potential-based model for undoped nano scale surrounding-gate MOSFETs. IEEE Trans Electron Devices, 2007, 54(9): 2193
[35] He J, Zhang J, Zhang L, et al. A surface potential based non-charge-sheet core model for undoped surrounding-gate MOSFETs. Journal of Semiconductors, 2009, 30(2): 024001
[36] Ortiz-Conde A, Garcia Sanchez F J, Guzman M. Exact analytical solution of channel surface potential as an explicit function of gate voltage in undoped-body MOSFETs using the Lambert-W function and a threshold voltage definition therefrom. Solid State Electron, 2003, 47(11): 2067
[37] He J, Fang M, Li B, et al. A new analytical approximation to general diode equation. Solid State Electron, 2006, 50(8): 1371
[38] TCAD Sentaurus Device User's Manual. Mountain View, CA: Synopsys, 2008